NACA

AUTHOR'S PERSONAL COPY

RESEARCH MEMORANDUM

AN INVESTIGATION OF A SUPERSONIC AIRCRAFT CONFIGURATION

HAVING A TAPERED WING WITH CIRCULAR-ARC SECTIONS AND 40° SWEEPBACK

STATIC LATERAL CONTROL CHARACTERISTICS AT

MACH NUMBERS OF 1.40 AND 1.59

By Ross B. Robinson

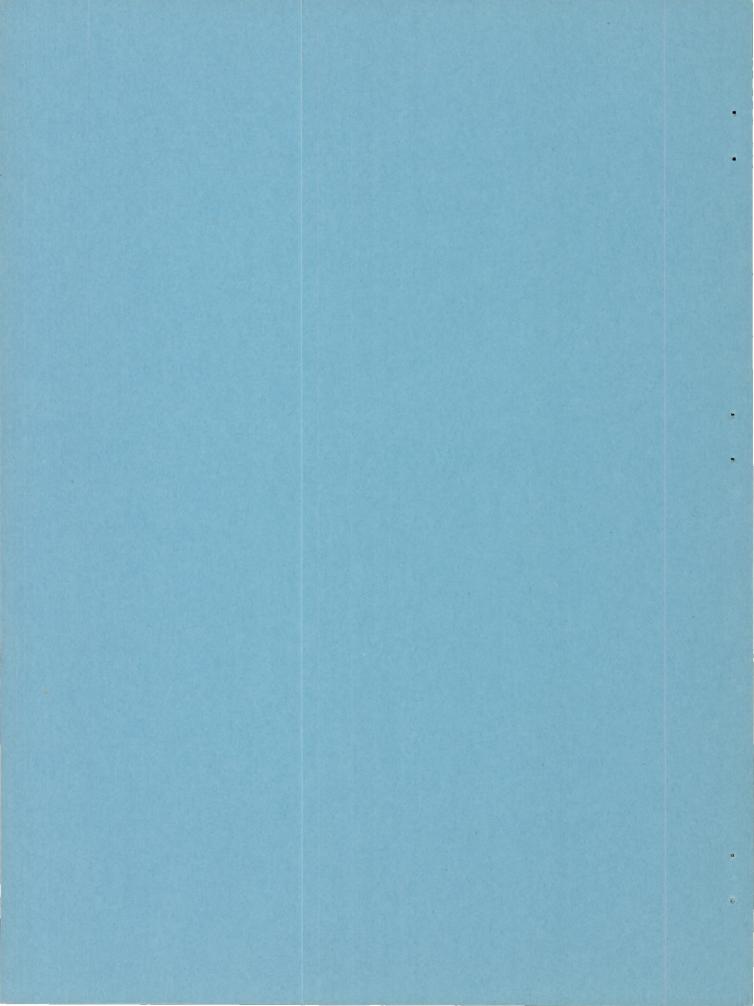
Langley Aeronautical Laboratory Langley Air Force Base. Va.

CLASSIFIED DOCUMENT

document contains classified information affecting the National Defense of the United S ag of the Espionage Act, USC 50:31 and 32. Its transmission or the revelation of its r to an unauthorized person is prohibited by law. mation so classified may be imparted only to persons in the military and naval servic appropriate civilian officers and employees of the Federal Government who have a leg and to United States citizens of known loyalty and discretion who of necessity must be in

NATIONAL ADVISORY COMMITTEE FOR AERONAUTICS

WASHINGTON November 10, 1950



NATIONAL ADVISORY COMMITTEE FOR AERONAUTICS

RESEARCH MEMORANDUM

AN INVESTIGATION OF A SUPERSONIC AIRCRAFT CONFIGURATION

HAVING A TAPERED WING WITH CIRCULAR-ARC SECTIONS AND 40° SWEEPBACK

STATIC LATERAL CONTROL CHARACTERISTICS AT

MACH NUMBERS OF 1.40 AND 1.59

By Ross B. Robinson

SUMMARY

An investigation has been conducted in the Langley 4- by 4-foot supersonic tunnel to determine the static lateral control characteristics of a supersonic aircraft configuration at Mach numbers of 1.40 and 1.59. The results indicated the aileron effectiveness to be approximately half that predicted by linear theory principally as a result of flow separation in the region of the aileron. The rudder effectiveness was considered low since a rudder deflection of approximately 20° produced a sideslip angle of only 2.5° at the test Mach numbers. The effective dihedral was positive with controls fixed. However, the variation of rolling-moment coefficient with angle of yaw for zero yawing moment indicated a dihedral effect that was slightly negative at a Mach number of 1.40 and slightly positive at a Mach number of 1.59.

A discussion of the accuracy of the strain-gage balance system used is included in an appendix.

INTRODUCTION

A comprehensive wind-tunnel investigation has been conducted in the Langley 4- by 4-foot supersonic tunnel to determine the general aerodynamic characteristics as well as the stability and control characteristics of a supersonic aircraft configuration. The geometric characteristics and a three-view drawing of the model are presented in table I and figure 2, respectively.

The longitudinal stability and control characteristics of the model are presented in references 1 and 2 for Mach numbers of 1.40 and 1.59, respectively. Lateral stability characteristics are presented in reference 3. Pressure measurements over the fuselage of the model are presented in reference 4 for a Mach number of 1.40 and in reference 5 for a Mach number of 1.59. Wing pressure measurements for a Mach number of 1.59 are given in reference 6.

The present paper contains the results of the lateral-control investigation conducted at Mach numbers of 1.40 and 1.59. The model incorporated a six-component internal strain-gage balance and hingemoment gages on the stabilizer, aileron, and rudder. Lateral control characteristics are presented for the complete model through a range of angles of attack and yaw for various aileron and rudder deflections.

COEFFICIENTS AND SYMBOLS

The results of the tests are presented as standard NACA coefficients of forces and moments. The data are referred to the stability axes system (fig. 1) with the reference center of gravity at 25 percent of the mean aerodynamic chord.

The coefficients and symbols are defined as follows:

CL	lift coefficient (Lift/qS where Lift = $-Z$)
c_{X}	longitudinal-force coefficient (X/qS)
CY	lateral-force coefficient (Y/qS)
Cl	rolling-moment coefficient (L/qSb)
Cm	pitching-moment coefficient $(M'/qS\overline{c})$
Cn	yawing-moment coefficient (N/qSb)
Cha	aileron hinge-moment coefficient $\left(H_{a}/2M_{a}q\right)$
Chr	rudder hinge-moment coefficient $\left(\mathrm{H_r/2M_{rq}}\right)$
X	force along X-axis, pounds
Y	force along Y-axis, pounds
Z	force along Z-axis, pounds

L moment about X-axis, pound-feet M' moment about Y-axis, pound-feet N moment about Z-axis, pound-feet Ha aileron hinge moment, pound-feet Hr rudder hinge moment, pound-feet S wing area, square feet Ma moment area of aileron about hinge line, feet ³ Mr moment area of rudder about hinge line, feet ³ b wing span, feet C wing mean aerodynamic chord, feet (\frac{2}{S}\int_0^{b/2} c^2 \dy) c airfoil section chord, feet y distance along wing span, feet q free-stream dynamic pressure, pounds per square foot M Mach number V airspeed, feet per second α angle of attack of fuselage center line, degrees ψ angle of yaw, degrees δar right-aileron deflection with respect to wing chord measure in stream direction, degrees δr rudder deflection with respect to vertical tail chord measured in stream direction, degrees Cyψ rate of change of lateral-force coefficient with angle of yaw, per degree (\frac{\partial Cy}{\partial Cy}\partial \partial \text{vist} and \text{vist} a		
Moment about Z-axis, pound-feet Ha aileron hinge moment, pound-feet Hr rudder hinge moment, pound-feet S wing area, square feet Ma moment area of aileron about hinge line, feet ³ Mr moment area of rudder about hinge line, feet ³ b wing span, feet C wing mean aerodynamic chord, feet (2/S) ∫ 0 c²dy) c airfoil section chord, feet y distance along wing span, feet q free-stream dynamic pressure, pounds per square foot M Mach number V airspeed, feet per second angle of attack of fuselage center line, degrees y angle of yaw, degrees δaR right-aileron deflection with respect to wing chord measured in stream direction, degrees δr rudder deflection with respect to vertical tail chord measured in stream direction, degrees Cyψ rate of change of lateral-force coefficient with angle of yaw, per degree (∂Cy/∂ψ) Choa rate of change of aileron hinge-moment coefficient with	L	moment about X-axis, pound-feet
Ha aileron hinge moment, pound-feet Hr rudder hinge moment, pound-feet S wing area, square feet Ma moment area of aileron about hinge line, feet ³ Mr moment area of rudder about hinge line, feet ³ b wing span, feet C wing mean aerodynamic chord, feet (\frac{2}{S}\int_0^{b/2} c^2 \text{dy}) c airfoil section chord, feet y distance along wing span, feet free-stream dynamic pressure, pounds per square foot M Mach number V airspeed, feet per second angle of attack of fuselage center line, degrees angle of yaw, degrees \(\text{bar} \) angle of yaw, degrees \(\text{car} \) right-aileron deflection with respect to wing chord measured in stream direction, degrees \(\text{cr} \) rudder deflection with respect to vertical tail chord measured in stream direction, degrees \(\text{Cy} \) rate of change of lateral-force coefficient with angle of yaw, per degree (\text{OCy}\sqrt{\text{dy}}) \(\text{dy} \)) Choa rate of change of aileron hinge-moment coefficient with	M '	moment about Y-axis, pound-feet
Hr rudder hinge moment, pound-feet S wing area, square feet Ma moment area of aileron about hinge line, feet ³ Mr moment area of rudder about hinge line, feet ³ b wing span, feet c wing mean aerodynamic chord, feet (2/S) (2/O) c ² dy) c airfoil section chord, feet y distance along wing span, feet q free-stream dynamic pressure, pounds per square foot M Mach number V airspeed, feet per second angle of attack of fuselage center line, degrees w angle of yaw, degrees δar right-aileron deflection with respect to wing chord measured in stream direction, degrees δr rudder deflection with respect to vertical tail chord measured in stream direction, degrees Cyψ rate of change of lateral-force coefficient with angle of yaw, per degree (∂Cy/∂ψ) Chδa rate of change of aileron hinge-moment coefficient with	N	moment about Z-axis, pound-feet
moment area of aileron about hinge line, feet ³ Mr moment area of rudder about hinge line, feet ³ b wing span, feet wing span, feet airfoil section chord, feet distance along wing span, feet free-stream dynamic pressure, pounds per square foot M Mach number v airspeed, feet per second angle of attack of fuselage center line, degrees angle of yaw, degrees angle of yaw, degrees right-aileron deflection with respect to wing chord measure in stream direction, degrees rudder deflection with respect to vertical tail chord measured in stream direction, degrees rate of change of lateral-force coefficient with angle of yaw, per degree (∂Cy/∂Ψ) change rate of change of aileron hinge-moment coefficient with	Ha	aileron hinge moment, pound-feet
Ma moment area of aileron about hinge line, feet ³ Mr moment area of rudder about hinge line, feet ³ b wing span, feet c wing mean aerodynamic chord, feet (² / _S ∫ ₀ ^{b/2} c ² dy) c airfoil section chord, feet y distance along wing span, feet q free-stream dynamic pressure, pounds per square foot M Mach number V airspeed, feet per second α angle of attack of fuselage center line, degrees ψ angle of yaw, degrees δaR right-aileron deflection with respect to wing chord measured in stream direction, degrees δr rudder deflection with respect to vertical tail chord measured in stream direction, degrees Cyψ rate of change of lateral-force coefficient with angle of yaw, per degree (∂Cy/∂Ψ) Chδa rate of change of aileron hinge-moment coefficient with	Hr	rudder hinge moment, pound-feet
Mr moment area of rudder about hinge line, feet ³ b wing span, feet c wing mean aerodynamic chord, feet $\left(\frac{2}{S}\int_0^{b/2}c^2\mathrm{dy}\right)$ c airfoil section chord, feet y distance along wing span, feet q free-stream dynamic pressure, pounds per square foot M Mach number V airspeed, feet per second α angle of attack of fuselage center line, degrees ψ angle of yaw, degrees δaR right-aileron deflection with respect to wing chord measured in stream direction, degrees c rudder deflection with respect to vertical tail chord measured in stream direction, degrees c rate of change of lateral-force coefficient with angle of yaw, per degree (∂Cy/∂Ψ) Chδa rate of change of aileron hinge-moment coefficient with	S	wing area, square feet
wing span, feet wing mean aerodynamic chord, feet $\left(\frac{2}{S}\int_0^{b/2}c^2dy\right)$ c airfoil section chord, feet y distance along wing span, feet q free-stream dynamic pressure, pounds per square foot M Mach number V airspeed, feet per second angle of attack of fuselage center line, degrees w angle of yaw, degrees bar right-aileron deflection with respect to wing chord measured in stream direction, degrees crudder deflection with respect to vertical tail chord measured in stream direction, degrees cy rate of change of lateral-force coefficient with angle of yaw, per degree $(\partial C_y/\partial \Psi)$ Choa rate of change of aileron hinge-moment coefficient with	Ma	moment area of aileron about hinge line, feet ³
wing mean aerodynamic chord, feet $\left(\frac{2}{S}\int_0^{b/2}c^2\mathrm{dy}\right)$ c airfoil section chord, feet y distance along wing span, feet q free-stream dynamic pressure, pounds per square foot M Mach number V airspeed, feet per second α angle of attack of fuselage center line, degrees ψ angle of yaw, degrees δaR right-aileron deflection with respect to wing chord measured in stream direction, degrees δr rudder deflection with respect to vertical tail chord measured in stream direction, degrees Cyψ rate of change of lateral-force coefficient with angle of yaw, per degree (∂Cy/∂ψ) Chδa rate of change of aileron hinge-moment coefficient with	Mr	moment area of rudder about hinge line, feet ³
c airfoil section chord, feet y distance along wing span, feet q free-stream dynamic pressure, pounds per square foot M Mach number V airspeed, feet per second α angle of attack of fuselage center line, degrees ψ angle of yaw, degrees δaR right-aileron deflection with respect to wing chord measured in stream direction, degrees δr rudder deflection with respect to vertical tail chord measured in stream direction, degrees Cyψ rate of change of lateral-force coefficient with angle of yaw, per degree (∂Cy/∂ψ) Chδa rate of change of aileron hinge-moment coefficient with	ъ	wing span, feet
y distance along wing span, feet q free-stream dynamic pressure, pounds per square foot M Mach number V airspeed, feet per second α angle of attack of fuselage center line, degrees ψ angle of yaw, degrees δaR right-aileron deflection with respect to wing chord measured in stream direction, degrees δr rudder deflection with respect to vertical tail chord measured in stream direction, degrees Cyψ rate of change of lateral-force coefficient with angle of yaw, per degree (∂Cy/∂Ψ) Chδa rate of change of aileron hinge-moment coefficient with	c	wing mean aerodynamic chord, feet $\left(\frac{2}{S}\int_{0}^{b/2}c^{2}dy\right)$
free-stream dynamic pressure, pounds per square foot M Mach number V airspeed, feet per second α angle of attack of fuselage center line, degrees ψ angle of yaw, degrees δaR right-aileron deflection with respect to wing chord measured in stream direction, degrees δr rudder deflection with respect to vertical tail chord measured in stream direction, degrees Cyψ rate of change of lateral-force coefficient with angle of yaw, per degree (∂Cy/∂ψ) Chδa rate of change of aileron hinge-moment coefficient with	С	airfoil section chord, feet
M Mach number V airspeed, feet per second α angle of attack of fuselage center line, degrees ψ angle of yaw, degrees δaR right-aileron deflection with respect to wing chord measured in stream direction, degrees δr rudder deflection with respect to vertical tail chord measured in stream direction, degrees Cyψ rate of change of lateral-force coefficient with angle of yaw, per degree (∂Cy/∂ψ) Chδa rate of change of aileron hinge-moment coefficient with	У	distance along wing span, feet
V airspeed, feet per second α angle of attack of fuselage center line, degrees ψ angle of yaw, degrees δaR right-aileron deflection with respect to wing chord measured in stream direction, degrees δr rudder deflection with respect to vertical tail chord measured in stream direction, degrees Cyψ rate of change of lateral-force coefficient with angle of yaw, per degree (∂Cy/∂ψ) Chδa rate of change of aileron hinge-moment coefficient with	q	free-stream dynamic pressure, pounds per square foot
 angle of attack of fuselage center line, degrees ψ angle of yaw, degrees δaR right-aileron deflection with respect to wing chord measured in stream direction, degrees δr rudder deflection with respect to vertical tail chord measured in stream direction, degrees Cyψ rate of change of lateral-force coefficient with angle of yaw, per degree (∂Cy/∂ψ) Chδa rate of change of aileron hinge-moment coefficient with 	М	Mach number
 ψ angle of yaw, degrees δaR right-aileron deflection with respect to wing chord measured in stream direction, degrees δr rudder deflection with respect to vertical tail chord measured in stream direction, degrees Cyψ rate of change of lateral-force coefficient with angle of yaw, per degree (∂Cy/∂ψ) Chδa rate of change of aileron hinge-moment coefficient with 	V	airspeed, feet per second
 δaR right-aileron deflection with respect to wing chord measured in stream direction, degrees δr rudder deflection with respect to vertical tail chord measured in stream direction, degrees Cyψ rate of change of lateral-force coefficient with angle of yaw, per degree (∂Cy/∂Ψ) Chδa rate of change of aileron hinge-moment coefficient with 	a	angle of attack of fuselage center line, degrees
 Stream direction, degrees rudder deflection with respect to vertical tail chord measured in stream direction, degrees Cyψ rate of change of lateral-force coefficient with angle of yaw, per degree (∂Cy/∂ψ) Chδa rate of change of aileron hinge-moment coefficient with 	Ψ	angle of yaw, degrees
measured in stream direction, degrees $ ^{\text{C}} y_{\psi} $	δ_{a_R}	right-aileron deflection with respect to wing chord measured in stream direction, degrees
Choa rate of change of aileron hinge-moment coefficient with	$\delta_{\mathbf{r}}$	
	$^{\mathrm{C}}\mathbf{y}_{\psi}$	
	Choa	

Chor	rate of change of rudder hinge-moment coefficient with rudder deflection, per degree $\left(\partial C_{h_r}/\partial \delta_r\right)$
$c_{ha_{\alpha}}$	rate of change of aileron hinge-moment coefficient with angle of attack, per degree $\left(\partial C_{\rm h_a}/\partial\alpha\right)$
$^{\mathrm{Ch}_{\mathrm{r}_{\psi}}}$	rate of change of rudder hinge-moment coefficient with angle of yaw, per degree $\left(\partial C_{h_T}/\partial \Psi\right)$
Cloa	rate of change of rolling-moment coefficient with aileron deflection, per degree $\left(\partial C_l/\partial \delta_{a_R}\right)$
C _{nδ} r	rate of change of yawing-moment coefficient with rudder deflection, per degree $\left(\partial C_n \middle/ \partial \delta_r\right)$
Clp	rate of change of rolling-moment coefficient with rolling velocity, per radian $\left(\partial C_{l}/\partial \frac{pb}{2V}\right)$
pb 2V	wing-tip helix angle, radians (C_l/C_{lp})
р	rolling velocity, radians per second
	ollowing symbols appear only in the appendix:
The f	ollowing symbols appear only in the appendix:
The f $C_{\mathbb{C}}$	ollowing symbols appear only in the appendix: chord-force coefficient (C/qS)
The f $^{\text{C}}_{\text{C}}$	ollowing symbols appear only in the appendix: chord-force coefficient (C/qS) normal-force coefficient (N'/qS)
The f CC CN Cht	ollowing symbols appear only in the appendix: chord-force coefficient (C/qS) normal-force coefficient (N'/qS) stabilizer hinge-moment coefficient $(H_t/S_t\overline{c}_tq)$
The f CC CN Cht	chord-force coefficient (C/qS) normal-force coefficient (N'/qS) stabilizer hinge-moment coefficient ($H_t/S_t\overline{c}_tq$) chord force, pounds
The f CC CN Cht C	chord-force coefficient (C/qS) normal-force coefficient (N'/qS) stabilizer hinge-moment coefficient (Ht/Stctq) chord force, pounds normal force, pounds
The f CC CN Cht C N' Ht	chord-force coefficient (C/qS) normal-force coefficient (N'/qS) stabilizer hinge-moment coefficient (Ht/Stctq) chord force, pounds normal force, pounds stabilizer hinge moment, pound-feet area of stabilizer, square feet
The f	chord-force coefficient (C/qS) normal-force coefficient (N'/qS) stabilizer hinge-moment coefficient (Ht/Stctq) chord force, pounds normal force, pounds stabilizer hinge moment, pound-feet

yt distance along stabilizer span, feet

it stabilizer incidence angle with respect to fuselage center line, degrees

MODEL AND APPARATUS

A three-view drawing of the model is shown in figure 2 and the geometric characteristics of the model are given in table I. The model had a wing with 40° of sweepback of the quarter-chord line, aspect ratio 4, taper ratio 0.5, and 10-percent-thick circular-arc sections normal to the quarter-chord line. The wing was at a 3° incidence angle with respect to the fuselage center line. Twenty-percent-chord flat-sided ailerons having a trailing-edge thickness 0.5 of the hinge-line thickness were installed on the outboard halves of the wing semispans (fig. 3). Measurements indicated the right wing tip to be twisted +0.2° with respect to the left wing tip.

Details of the vertical tail and rudder are shown in figure 4. Deflections of the right aileron and the rudder were set manually before each run.

The model was mounted on a sting support and its angle in the horizontal plane was remotely controlled in such a manner that the model remained essentially in the center of the test section. With the model mounted so that the wings were vertical, tests could be made through an angle-of-attack range. (See fig. 5(a).) With the model rotated 90° (wings horizontal), the angle-of-attack mechanism was used to provide angles of yaw (fig. 5(b)). At M=1.40, a 6° bent sting was used for all pitch tests except $\delta_{\rm aR}=0^{\circ}$ in which case the straight sting was used. The yaw tests at M=1.40 and both pitch and yaw tests at M=1.59 were made using the straight (0°) sting. Comparison of the results of runs made using various bent stings indicated that any sting effects are not affected by the shape of the stings used in these tests.

Forces and moments on the model were measured by means of an internal six-component strain-gage balance. Aileron and rudder hinge moments were measured by individual strain-gage beams in each control surface. A discussion of the balance system and the accuracy of the data are given in the appendix.

The tests were conducted in the Langley 4- by 4-foot supersonic tunnel which is described in reference 5.

TEST CONDITIONS

The test conditions are summarized in the following table:

Mach number	Stagnation pressure (atm)	Stagnation temperature (°F)	Dew point (OF)	Dynamic pressure (lb/sq ft)	Reynolds number (based on \overline{c})
1.40	0.25	110	-30	229	600,000
1.59	.25	110	-35	223	575,000

Calibration data for the Mach number 1.40 and Mach number 1.59 nozzles are presented in references 4 and 5, respectively.

CORRECTIONS AND ACCURACY

Although it is believed that the sting effects were small, their exact magnitudes are not known. Base pressure measurements at a Mach number of 1.59 indicated that, if free-stream static pressure is assumed to exist at the base of the model, then the drag data presented would be reduced by approximately 1 percent in the angle-of-attack range from 4° to 10°, with no correction necessary in the lower angle range. No corrections for these effects have been made to the data. The maximum sting deflection under load was within the accuracy of the angle measurements, and no angle of attack or yaw correction was required. Optical measurements of the wing twist under load indicated twists of less than 0.05° and hence no corrections for aeroelastic effects were necessary. No wing-twist measurements were made with the aileron deflected.

The probable errors in the aerodynamic coefficients (see appendix) are less than

								All balance-system and tunnel errors combined			
CL.										±0.0010	±0.0043
CX .										±.00025	±.0023
CY .										±.0010	±.0019
Cm.										±.00045	±.0014
Cn.										±.00011	±.00015
CZ.										±.00006	±.000099
Cha										±.0028	±.0031
Ch_r										±.0027	±.0028

where random balance-system errors include zero shift and sensitivity only.

The accuracy of the angle of attack and angle of yaw was about $\pm 0.05^{\circ}$, the rudder and aileron deflection angles about $\pm 0.05^{\circ}$, and the dynamic pressure about 0.25 percent.

Because of the small magnitudes of the flow gradient in the vicinity of the model (references 4 and 5), no corrections for these effects have been applied. Tests made with the model in a horizontal and vertical position showed excellent agreement.

TEST PROCEDURE

Aileron tests were made through an angle-of-attack range of -4° to 10° at zero angle of yaw with a right-aileron-deflection range of about $\pm 15^{\circ}$. The left aileron remained at zero deflection throughout the tests. The aileron tests were made using various stabilizer deflections so that the model remained trimmed in pitch. Rudder tests were made through a yaw-angle range of $\pm 10^{\circ}$ at zero angle of attack. The rudder-deflection ranges were -3° to 20° for M = 1.40 and -3° to 25.5° for M = 1.59.

RESULTS AND DISCUSSION

Aileron Characteristics

The aerodynamic characteristics of the complete model for various aileron deflections through the angle-of-attack range at Mach numbers of 1.40 and 1.59 are presented in figures 6 and 7, respectively. These data show the effects of deflecting the right aileron only. The negative rolling-moment coefficient indicated for zero aileron deflection at M = 1.40 (see fig. 6) can be attributed to the slight twist of the wing. At M = 1.59 (see fig. 7) the effects of the wing twist appear to be counteracted by flow angularities in the region of the aileron or by incorrect aileron setting.

The adverse yawing moment accompanying total aileron deflection is about the same at both Mach numbers and is approximately equal to that which occurs at low speeds for a similar configuration (reference 7).

The experimental and theoretical variations of the rolling-moment coefficient and aileron hinge-moment coefficient with aileron deflection for both Mach numbers are presented in figure 8. The experimental

results were obtained by cross plotting from figures 6 and 7 at zero angle of attack. The theoretical values of $c_{l\delta a}$ and $c_{h\delta a}$ were calculated by the methods presented in reference 8. An examination of figures 6 and 7 indicates that $c_{l\delta a}$ and $c_{h\delta a}$ are about constant for small aileron deflections throughout the angle-of-attack range.

At both Mach numbers, c_l and c_{ha} vary linearly with δ_{aR} through most of the deflection range and there is no indication of reversal in the aileron effectiveness. The values of $c_{l\delta_a}$ and $c_{h\delta_a}$ obtained experimentally are approximately half those predicted by linear theory, principally as a result of spanwise flow and boundary-layer separation in the region of the aileron. (See reference 6.)

A summary of the aileron characteristics $C_{h\delta_a}$, $C_{ha_{\alpha}}$, and $C_{l\delta_a}$ obtained from figures 6, 7, and 8 is presented in table II. All of these parameters are less at M=1.59 than at M=1.40. The aileron-effectiveness parameter $C_{l\delta_a}$ is about half the subsonic value of -0.00l indicated at M=0.16 for a model of the same configuration equipped with a circular-arc profile aileron (reference 7).

The rolling effectiveness pb/2V (fig. 9) was calculated using the experimental values of rolling-moment coefficient and the damping-in-roll factor C_{lp} obtained from the charts presented in reference 9. Values of pb/2V indicated by free-flight tests (reference 10) were about 0.8 of the calculated values, which probably results from the fact that the calculated results do not include the effects of adverse yaw. It is interesting to note that low-speed tests have indicated that an empirical correction factor of 0.8 is necessary to provide correlation between calculated and measured values of pb/2V (reference 11). The rolling velocities based on the model span (see fig. 9) indicate that at these Mach numbers reasonable rates of roll might be obtained for a full-scale airplane similar to the model.

Characteristics in Sideslip

<u>Directional control</u>.- The effects of rudder deflection on the aero-dynamic characteristics in yaw are presented in figures 10 and 11 for Mach numbers of 1.40 and 1.59, respectively.

As indicated in reference 3, the directional stability (Cn_{ψ}) at both Mach numbers is high relative to the low-speed value for this configuration. The rudder-free stability (dashed lines for $Ch_{\mathbf{r}}=0$ in figs. 10 and 11) indicates that, if the rudder is released at any yaw angle, the model would tend to return to zero yaw.

NACA RM L50Ill

Although low-speed tests (M = 0.16, reference 7) of a similar configuration indicate that reversal in $C_{h_{\Gamma_{\psi}}}$ occurs for small values of δ_{Γ} and $\psi,$ no reversal was found at either Mach number for the present tests.

The variation of rudder deflection with angle of yaw (fig. 12) obtained by cross plotting figures 10 and 11 at $C_n=0$ indicates that left-rudder deflection (positive δ_r) is required for right sideslip (negative ψ) and vice versa. The maximum rudder deflections (25.5° at M = 1.59 and 20° at M = 1.40) can hold a sideslip of about 2.5° at both Mach numbers. A considerably larger sideslip can be maintained at subsonic speeds, about 10° being attained for $\delta_r=20^\circ$ at M = 0.16 (reference 7). Rudder deflections of about 16° would be required to overcome the adverse yaw of about 1.5° (figs. 10 and 11) resulting from full aileron deflection ($\delta_a=\pm15^\circ$) at zero angle of attack.

Variations of yawing-moment and rudder hinge-moment coefficients with rudder deflection at zero angle of yaw, obtained by cross plotting figures 10 and 11, are presented in figure 13 for both Mach numbers. The rudder characteristics $C_{h\delta_r}$, $C_{h_{r\psi}}$, and $C_{n\delta_r}$ obtained from figures 10, 11, and 13 are presented in table II. The rudder-effectiveness parameter $C_{n\delta_r}$ is somewhat less at M = 1.59 than at M = 1.40 and is rather low compared to the subsonic value of -0.0010 at M = 0.16 (reference 7). The hinge-moment parameters $C_{h\delta_r}$ and $C_{h_{r\psi}}$ are also less at M = 1.59 than at M = 1.40.

Effective dihedral.- The variation of rolling-moment coefficient with angle of yaw with controls fixed (figs. 10 and 11) indicates positive effective dihedral at both Mach numbers. However, the variation of C_l with ψ for $C_n=0$ (dashed lines in figs. 10 and 11) indicates slightly negative effective dihedral at M=1.40 and positive effective dihedral at M=1.59, although these effects appear to be small at both Mach numbers. These results might be expected inasmuch as the tail-off tests (reference 3) have shown that all of the positive effective dihedral is contributed by the vertical tail. Hence, the effective dihedral probably would vary with rudder deflection.

Lateral characteristics in sideslip.— The positive value of the lateral-force parameter Cy_{ψ} indicates right bank will be required in steady right sideslip (figs. 10 and 11). The value of Cy_{ψ} is smaller at M = 1.59 than at M = 1.40 because of the reduced lift-curve slope of the vertical tail at M = 1.59 (reference 3).

Longitudinal characteristics in sideslip. There is little variation of lift coefficient and longitudinal-force coefficient with angle of yaw (figs. 10 and 11). The small variations of pitching-moment

coefficient with ψ and δ_r can easily be counteracted with only slight changes in stabilizer setting (references 1 and 2).

CONCLUSIONS

The results of the static-lateral-control investigation conducted at Mach numbers of 1.40 and 1.59 on a model of a supersonic aircraft configuration indicate the following conclusions:

- l. The aileron effectiveness was approximately half that predicted by linear theory principally as a result of flow separation in the region of the ailerons. However, an analysis of the results indicated that at these supersonic speeds the ailerons would produce reasonable rolling velocities for an airplane configuration similar to the model.
- 2. The rudder effectiveness at the test Mach numbers was considered low since a rudder deflection of approximately 20° produced a sideslip angle of only 2.5°.
- 3. With controls fixed the model had positive effective dihedral. However, the variation of rolling-moment coefficient with angle of yaw for zero yawing moment indicated a dihedral effect that was slightly negative at a Mach number of 1.40 and slightly positive at a Mach number of 1.59.
- 4. The adverse yawing moment that accompanied total aileron deflection was about the same at both Mach numbers and was about the same as that which occurred at low speeds for a similar configuration.

Langley Aeronautical Laboratory
National Advisory Committee for Aeronautics
Langley Air Force Base, Va.

APPENDIX

ESTIMATE OF BALANCE-SYSTEM ACCURACY

In an attempt to evaluate the performance of the six-component internal strain-gage balance and the three single-beam hinge-moment balances employed during the investigations of this model in the Langley 4- by 4-foot supersonic tunnel, a simplified analysis to determine the probable errors in the data and to indicate the sources of these errors is presented. This analysis includes uncertainties in flow parameters, angle settings, and model dimensions, as well as inaccuracies in the balance systems. The data used in this analysis have been determined from repeated calibrations and the results are presented as probable errors in the aerodynamic coefficients. In all cases, the errors considered are random errors except those errors introduced in the reduction of the data by neglecting interactions and slight calibration shifts. In the entire analysis, the balance system is considered to include the strain gages, wiring, control boxes, and the modified self-balancing potentiometers used as indicators.

Definition of Terms

- (a) Accuracy a measure of the ability of the balance system to indicate the correct reading for repeated applications of a given load
- (b) Sensitivity the smallest increment of load the system can detect and indicate
- (c) Zero shift the increment by which the indicator fails to return to the initial zero position after the load has been removed
- (d) Probable error the estimated magnitude of the net error to be expected in any single observation
- (e) Systematic error an error in which the sign and magnitude bear a fixed relation to the condition of observation
- (f) Random error an error in which the sign is as likely to be positive as negative
- (g) Interaction an increment in the reading of any given component caused by the application of one or more other components

Sources of Error

In the following analysis, the balance-system errors were first considered separately and later in combination with tunnel and model parameters to give an indication of the over-all reliability of the data. The balance-system errors considered were zero shift, recording sensitivity, calibration changes, and interactions. In evaluating the errors introduced by the tunnel and model parameters, such items as inaccuracies in angle of attack, angle of yaw, control-surface deflections, and free-stream dynamic pressure have been included. All the errors treated were of a random nature with the exception of the calibration shifts and interactions. These latter errors were systematic.

In general, all data used in analyzing the balance-system inaccuracies were obtained with the balances in place in the model during the period of the basic aerodynamic tests. The only exceptions involved were the interaction data which were obtained during final bench calibrations prior to installation in the tunnel.

ANALYSIS

In combining the various errors, the methods discussed in chapter III of reference 12 were followed and are briefly reviewed. If, for example, the chord force is considered, then

$$C = CCqS$$

or

$$dC = qS dC_C + C_CS dq + C_Cq dS$$

and

$$\frac{dC}{dS} = dC_C + C_C \frac{dq}{q} + C_C \frac{dS}{S}$$
 (1)

If the symbol $\, r \,$ is used to designate the probable error in any item (for example, $r_q = dq$), then squaring both sides of (1) and neglecting all cross-product terms since, on the average, the cross product of two random errors is zero, the probable error in $\, C_C \,$ is

$$(P.E. in C_C)^2 = \frac{r_C^2}{(qS)^2} = (r_{C_C})^2 + (C_C)^2 \left(\frac{r_q^2}{q^2} + \frac{r_S^2}{S^2}\right)$$
(2)

The probable error in the area determination rg in equation (2) was estimated on the basis of construction tolerances to be negligible.

The problem of determining the probable errors is therefore reduced to one of evaluating

$$(P.E. in CC)^2 = rCC^2 + CC^2 \left(\frac{rq^2}{q^2}\right)$$
 (3)

Equation (3) is the general expression for the probable error in $C_{\mathbb{C}}$ and includes both random and systematic errors. It may be rewritten as

$$(P.E. in Cc)^2 = r_1^2 + r_2^2$$
 (4)

where r₁ and r₂ are the random and systematic errors, respectively. The systematic errors included are

- (a) Interactions
- (b) Calibration shifts

which may be combined algebraically as

$$r_2 = r_a + r_b \tag{5}$$

All other errors considered were random in nature. These items were

- (c) Zero shift
- (d) Sensitivity
- (e) Inaccuracies in angle of attack or yaw
- (f) Inaccuracies in angle of incidence of the stabilizer, aileron, or rudder
- (g) Inaccuracies in the measurement of the free-stream dynamic pressure

and are combined as follows

$$r_1^2 = r_c^2 + r_d^2 + r_e^2 + r_f^2 + r_g^2$$
 (6)

When the balance alone is considered, items (e), (f), and (g) are taken as zero. All of the errors are converted into coefficient form by means of the calibration curve slopes and aerodynamic parameters. The

results of equations (5) and (6) are combined by equation (4) to give the probable error in coefficient form to be expected in the component being considered.

RESULTS AND DISCUSSION

The results of the analysis are presented in tables III and IV. Table III presents the errors due to the balance alone, part A including zero shift and sensitivity only and part B containing the effects of these items plus calibration changes and maximum interactions encountered during the tests. In table IV the effects of tunnel- and model-parameter errors are combined with the balance-system errors from table III. Since the balance measured normal force and chord force, normal-force coefficient (CN) and chord-force coefficient (CC) are used instead of lift coefficient (CL) and drag coefficient (CD).

A comparison of tables III and IV shows that the inaccuracies in angle settings and dynamic pressure had a considerable effect on the probable errors in all the quantities measured. The effects of interactions and calibration shift on CC were significant when moderate amounts of positive lift and negative pitching moment were applied to the model. The errors in rolling-moment and yawing-moment coefficients were influenced about equally by calibration and interaction errors and by tunnel-parameter inaccuracies.

In general, the errors are quite small and do not significantly affect the data obtained during this investigation. The probable errors due to the interactions are conservative because the loading conditions chosen were those causing the maximum inaccuracies in those components most sensitive to interactions.

REFERENCES

- 1. Spearman, M. Leroy: An Investigation of a Supersonic Aircraft Configuration Having a Tapered Wing with Circular-Arc Sections and 40° Sweepback. Static Longitudinal Stability and Control Characteristics at a Mach Number of 1.40. NACA RM L9L08, 1950.
- 2. Spearman, M. Leroy, and Hilton, John H., Jr.: An Investigation of a Supersonic Aircraft Configuration Having a Tapered Wing with Circular-Arc Sections and 40^o Sweepback. Static Longitudinal Stability and Control Characteristics at a Mach Number of 1.59. NACA RM L50E12, 1950.
- 3. Spearman, M. Leroy: An Investigation of a Supersonic Aircraft Configuration Having a Tapered Wing with Circular-Arc Sections and 40° Sweepback. Static Lateral Stability Characteristics at Mach Numbers of 1.40 and 1.59. NACA RM L50Cl7, 1950.
- 4. Hasel, Lowell E., and Sinclair, Archibald R.: A Pressure-Distribution Investigation of a Supersonic-Aircraft Fuselage and Calibration of the Mach Number 1.40 Nozzle of the Langley 4- by 4-Foot Supersonic Tunnel. NACA RM L50Bl4a, 1950.
- 5. Cooper, Morton, Smith, Norman F., and Kainer, Julian H.: A Pressure Distribution Investigation of a Supersonic Aircraft Fuselage and Calibration of the Mach Number 1.59 Nozzle of the Langley 4- by 4-Foot Supersonic Tunnel. NACA RM L9E27a, 1949.
- 6. Cooper, Morton, and Spearman, M. Leroy: An Investigation of a Supersonic Aircraft Configuration Having a Tapered Wing with Circular-Arc Sections and 40° Sweepback. A Pressure-Distribution Study of the Aerodynamic Characteristics of the Wing at Mach Number 1.59. NACA RM L50C24, 1950.
- 7. Goodson, Kenneth W., and Comisarow, Paul: Lateral Stability and Control Characteristics of an Airplane Model Having a 42.8° Sweptback Circular-Arc Wing with Aspect Ratio 4.00, Taper Ratio 0.50, and Sweptback Tail Surfaces. NACA RM L7G31, 1947.
- 8. Kainer, Julian H., and Marte, Jack E.: Theoretical Supersonic Characteristics of Inboard Trailing-Edge Flaps Having Arbitrary Sweep and Taper. Mach Lines behind Flap Leading and Trailing Edges. NACA TN 2205, 1950.
- 9. Harmon, Sidney M., and Jeffreys, Isabella: Theoretical Lift and Damping in Roll of Thin Wings with Arbitrary Sweep and Taper at Supersonic Speeds. Supersonic Leading and Trailing Edges.
 NACA TN 2114, 1950.

- 10. Sandahl, Carl A.: Free-Flight Investigation at Transonic and Supersonic Speeds of the Rolling Effectiveness of Several Aileron Configurations on a Tapered Wing Having 42.7° Sweepback. NACA RM L8K23, 1949.
- 11. Kayten, Gerald G.: Analysis of Wind-Tunnel Stability and Control Tests in Terms of Flying Qualities of Full-Scale Airplanes.
 NACA Rep. 825, 1945.
- 12. Brunt, David: The Combination of Observations. Second ed., Cambridge Univ. Press, 1931.

3

TABLE I.- GEOMETRIC CHARACTERISTICS OF MODEL

Wing: Area, sq ft
line
Horizontal tail: Area, sq ft
Vertical tail: Area (exposed), sq ft
Fuselage: Fineness ratio (neglecting canopies)
Miscellaneous: Tail length from $\overline{c}/4$ wing to $\overline{c}t/4$ tail, ft 0.917 Tail height, wing semispans above fuselage center line 0.153

TABLE II.- VARIATION OF AILERON AND RUDDER
CHARACTERISTICS WITH MACH NUMBER

D	Mach r	number		
Parameter	1.40	1.59		
	Aileronl			
$c_{h\delta_a}$	-0.020	-0.0157		
$c_{\mathbf{h}_{\mathbf{a}_{\alpha}}}$	020	0163		
Chac Cloa	00056	00044		
	Rudder ²			
$\mathtt{Ch}_{\mathtt{S}_{\mathtt{r}}}$	-0.0080	-0.0031		
$c_{\mathbf{h_{r\psi}}}$	0058	0043		
$^{ extsf{Ch}_{ extsf{r}_{\psi}}}$ $^{ extsf{Ch}_{ extsf{r}_{\psi}}}$	00023	00019		

 $1_{\text{Measured at}} \delta_{\text{aR}} = 0^{\circ}, \quad \alpha = 0^{\circ}.$

NACA

²Measured at $\delta_r = 0^{\circ}$, $\psi = 0^{\circ}$.

TABLE III. - ERRORS IN MEASUREMENTS DUE TO BALANCES ALONE

 $\overline{\mathbb{V}}$ alues for errors are given only for those scale ranges actually used during the tes $\overline{\mathbb{U}}$. A. Errors resulting from zero shift and sensitivity

Comp.	CN	$C_{ t m}$	CC	CY ·	Cn	Cl	$c_{ t ht}$	C _{ha}	Chr
2	±0.0021	±0.00046						±0.0028	
3	±.0011	±.00045	±0.00025		±0.00011	±0.00006	±0.0013		±0.0027
4	±.0010	±.0002	±.00025	±0.0010	±.00011	±.00006	±.0013		±.0027

B. Errors resulting from zero shift, sensitivity, calibration shifts, and combined loads for maximum interaction

Comp.	CN	Cm	CC	CY	Cn	Cl	Cht	Cha	Chr
2	±0.0026	±0.00062						±0.0028	
3	±.0019	±.00061	±0.0019		±0.00019	±0.00011	±0.0013		±0.0028
4	±.0014	±.00051	±.0019	±0.0011	±.00012	±.000096	±.0013		±.0028



TABLE IV. - ERRORS IN MEASUREMENTS DUE TO BALANCES AND TUNNEL

A. Errors resulting from zero shift, sensitivity, tunnel, and model inaccuracies

Comp.	CN	$C_{\mathbf{m}}$	CC	CY	Cn	Cl	$\mathtt{c}_{\mathtt{ht}}$	Cha	$\mathtt{Ch}_{\mathtt{r}}$
2	±0.0046	±0.0014						±0.0031	
3	±.0042	±.0014	±0.0013		±0.00015	±0.000075	±0.0017		±0.0028
4	±.0041	±.0014	±.0013	±0.0018	±.00014	±.000075	±.0017		±.0028

B. Errors resulting from zero shift, sensitivity, calibration shifts, combined loads for maximum interaction, and tunnel and model inaccuracies

Comp.	$C_{\mathbf{N}}$	C _m	CC	$C_{\mathbf{Y}}$	Cn	Cl	$c_{ m ht}$	$c_{ m ha}$	$c_{ m h_r}$
2	±0.0049	±0.0014						±0.0031	
3	±.0045	±.0014	±0.0023		±0.00021	±0.00013	±0.0017		±0.0028
14	±.0043	±.0014	±.0023	±0.0019	±.00015	±.000099	±.0017		±.0028

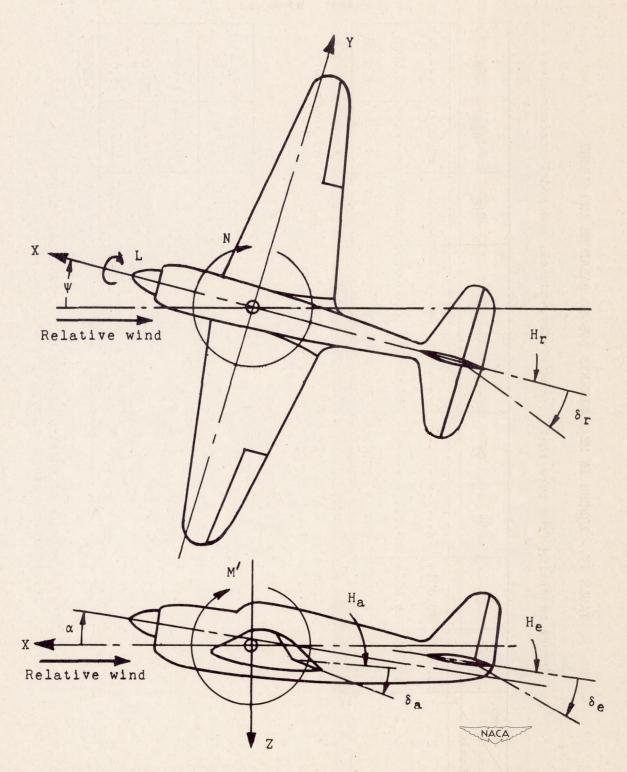


Figure 1.- System of axes and control-surface hinge moments and deflections. Positive values of forces, moments, and angles are indicated by arrows.

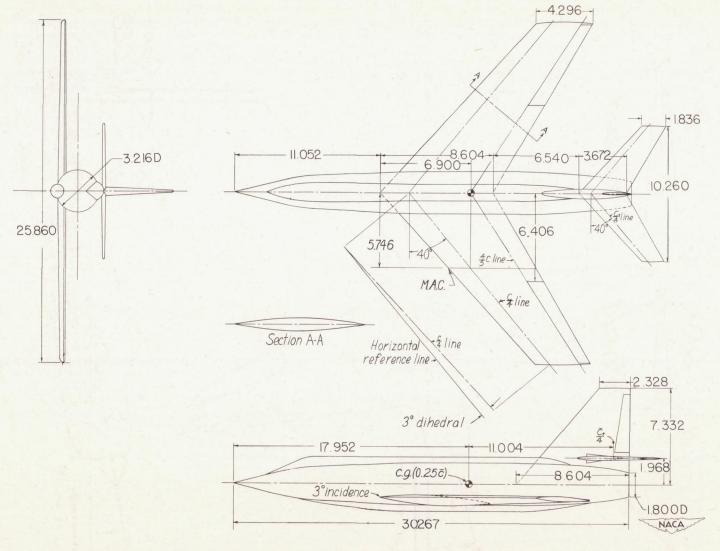


Figure 2.- Details of model of supersonic aircraft configuration.

Dimensions are in inches unless otherwise noted.

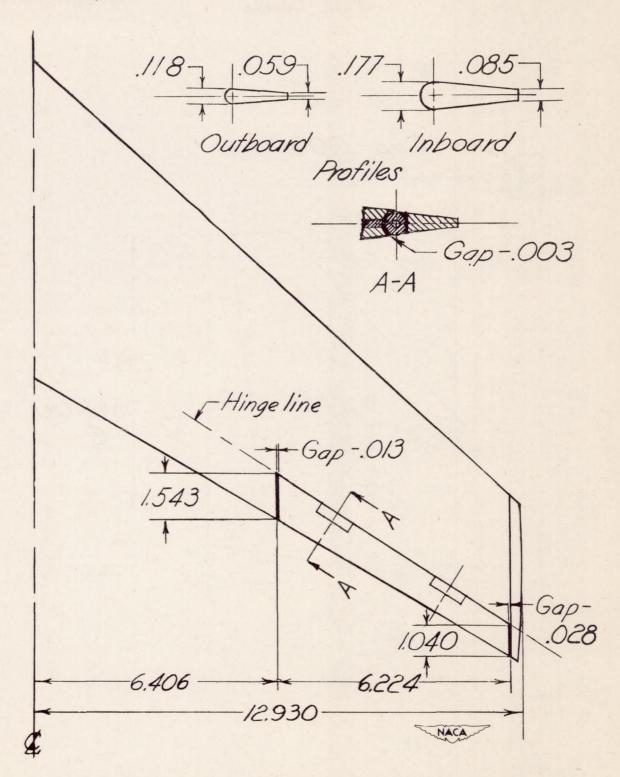


Figure 3.- Detail of wing semispan. All dimensions are in inches.

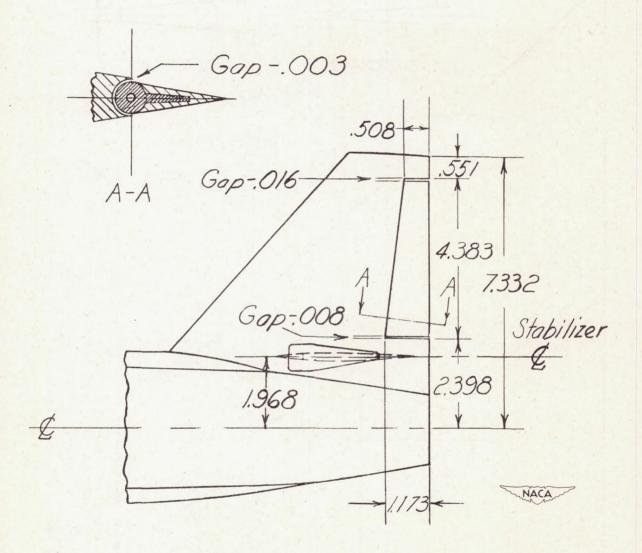
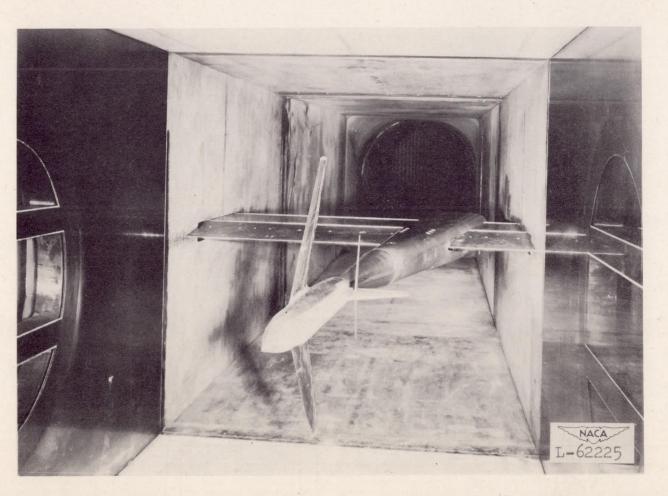
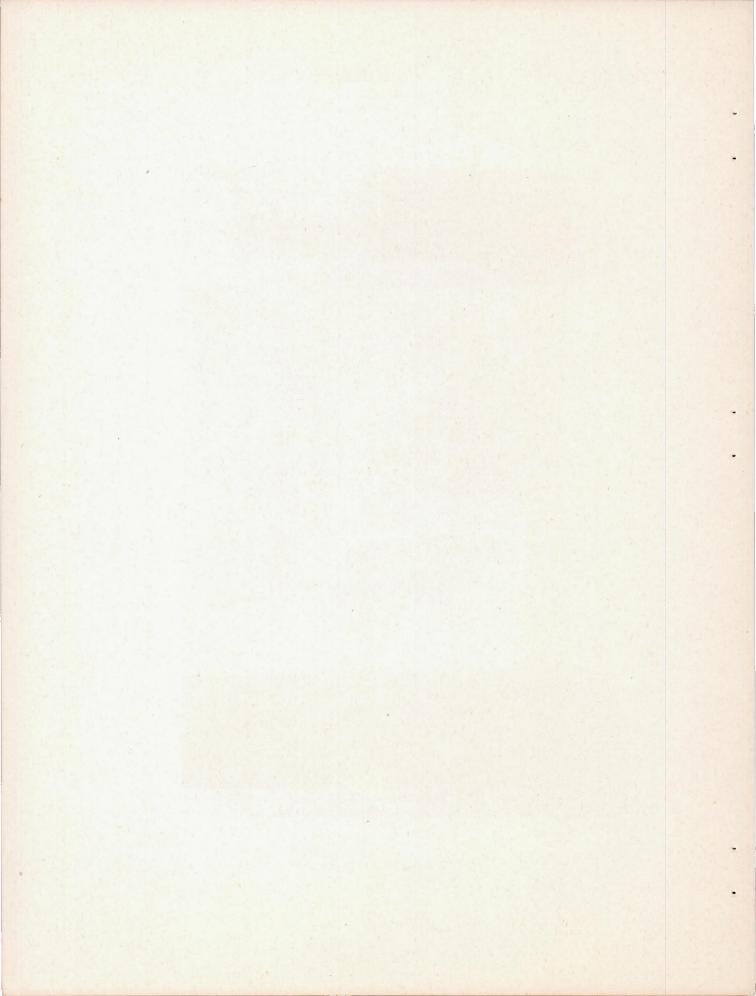


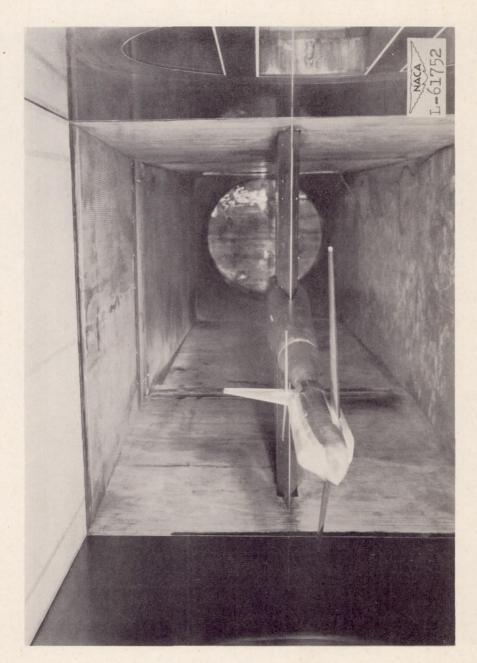
Figure 4. - Detail of vertical tail. All dimensions are in inches.



(a) Mounted for pitch tests. $\alpha = -10^{\circ}$; $\psi = 0^{\circ}$.

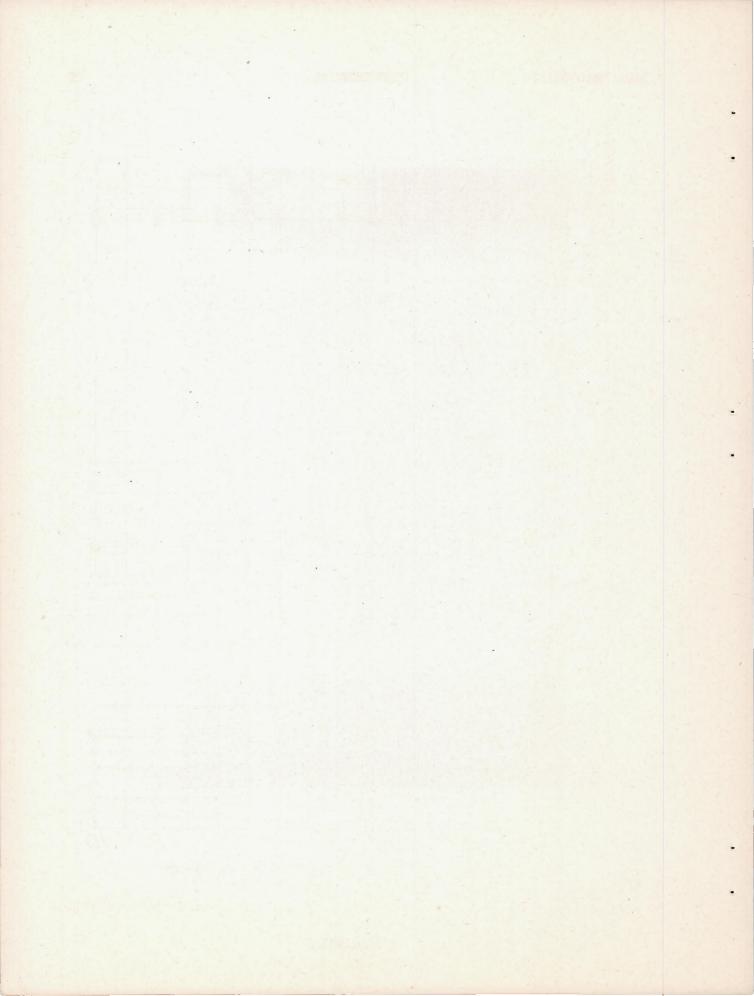
Figure 5.- Complete model of aircraft mounted in the Langley 4- by 4-foot supersonic tunnel.





(b) Mounted for yaw tests. $\alpha = 0^{\circ}$; $\psi = 0^{\circ}$.

Figure 5.- Concluded.



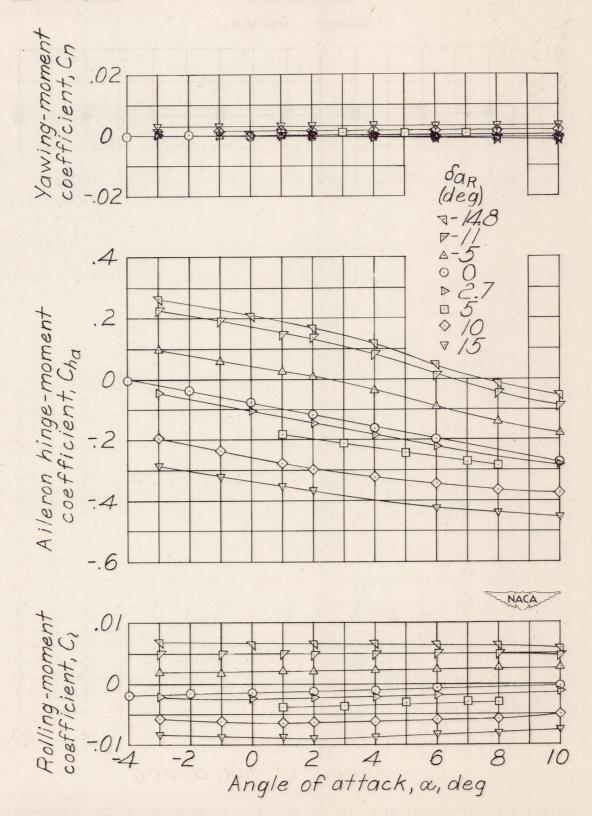


Figure 6.- Effect of aileron deflection on the aerodynamic characteristics in pitch. M = 1.40.

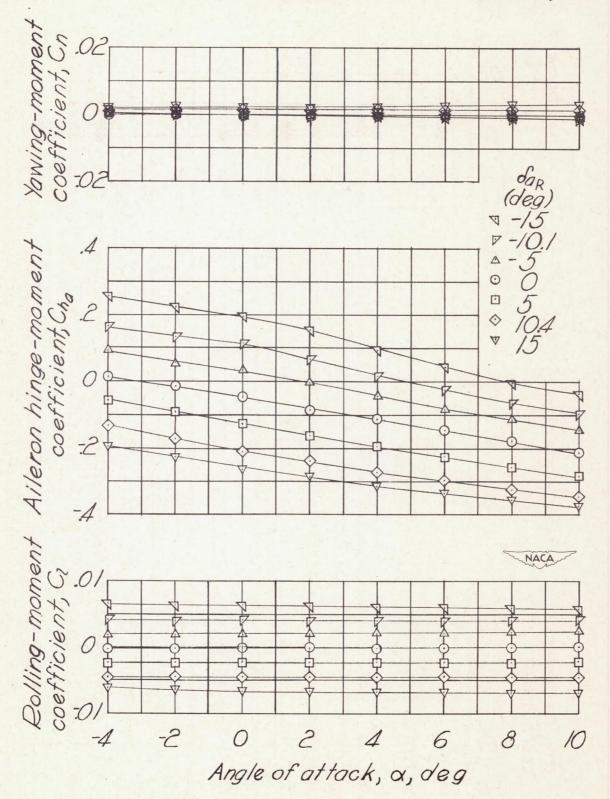


Figure 7.- Effect of aileron deflection on the aerodynamic characteristics in pitch. M = 1.59.

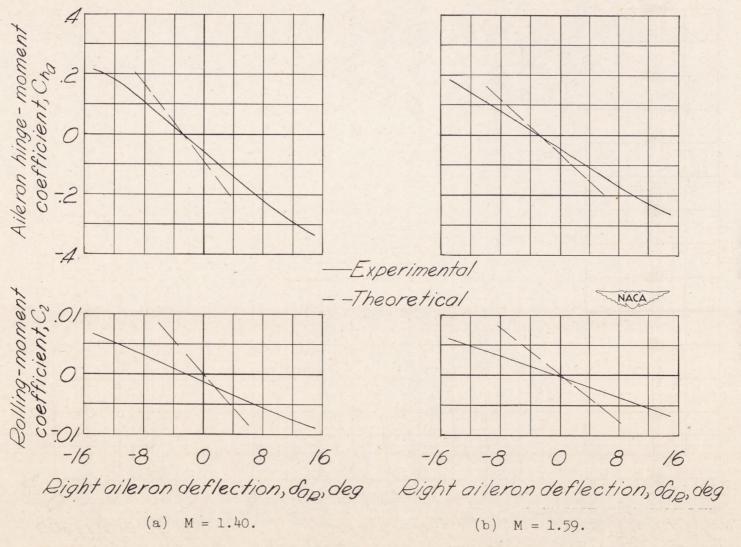


Figure 8.- Variation of rolling-moment and aileron hinge-moment coefficients with aileron deflection. $\alpha = 0^{\circ}$.

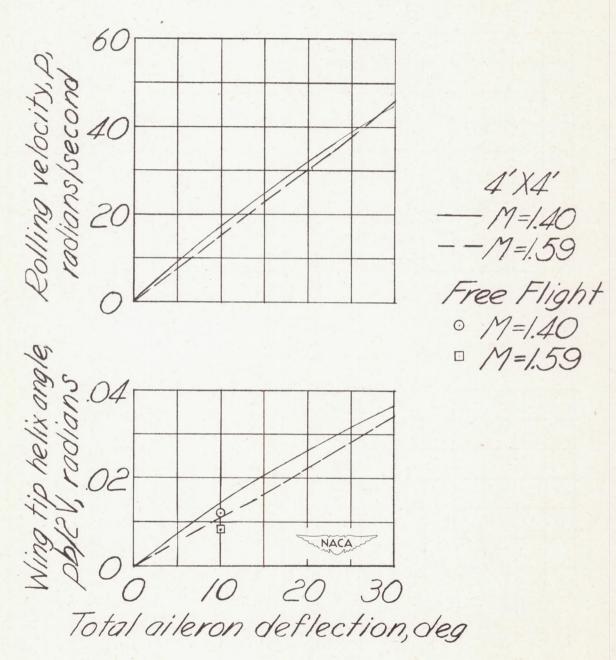


Figure 9.- Rolling characteristics of the model, $\alpha = 0^{\circ}$.

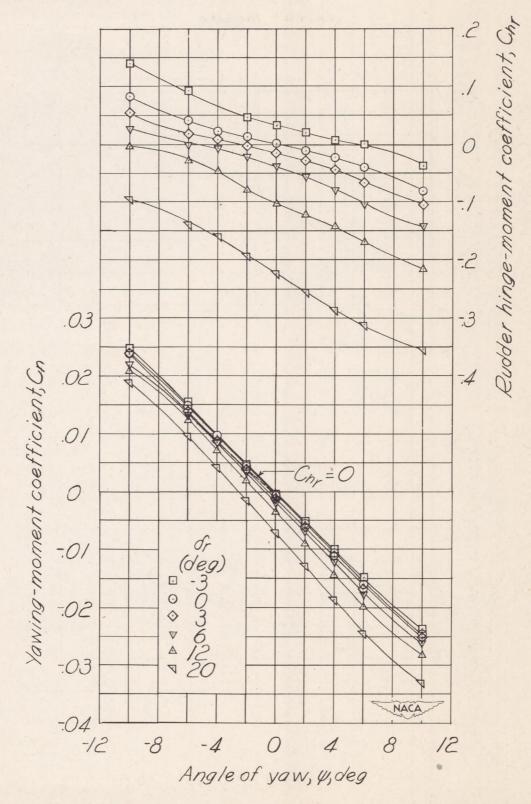


Figure 10.- Effect of rudder deflection on the aerodynamic characteristics in yaw. $\alpha = 0^{\circ}$, M = 1.40.

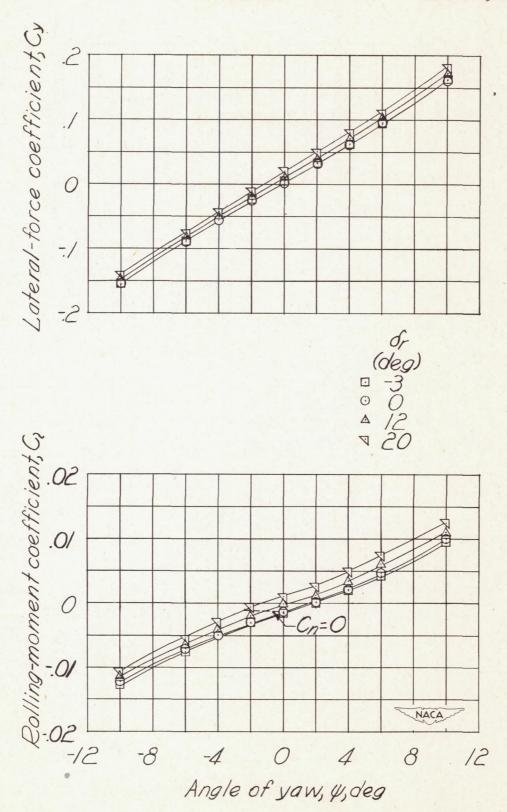
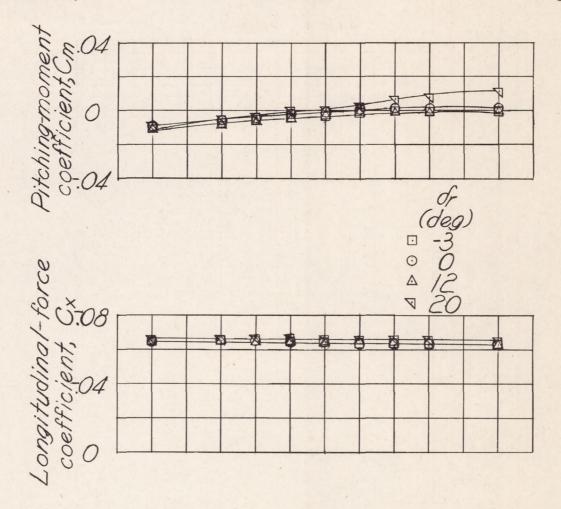


Figure 10. - Continued.



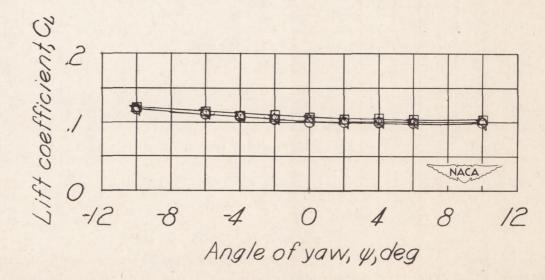


Figure 10. - Concluded.

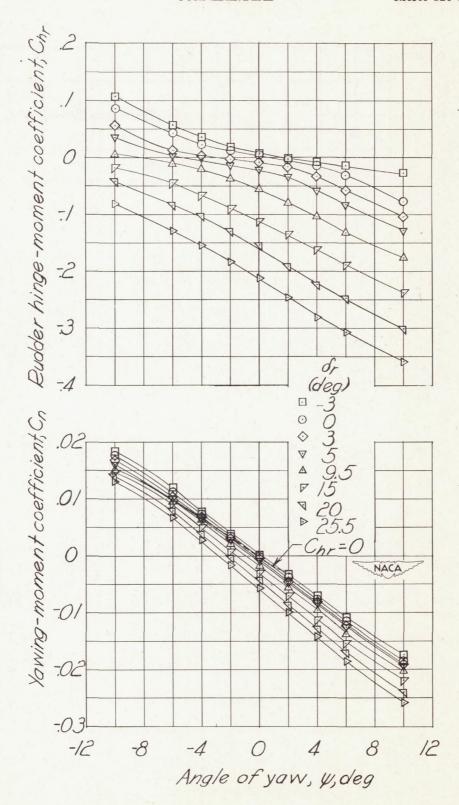


Figure 11.- Effect of rudder deflection on the aerodynamic characteristics in yaw. $\alpha = 0^{\circ}$, M = 1.59.

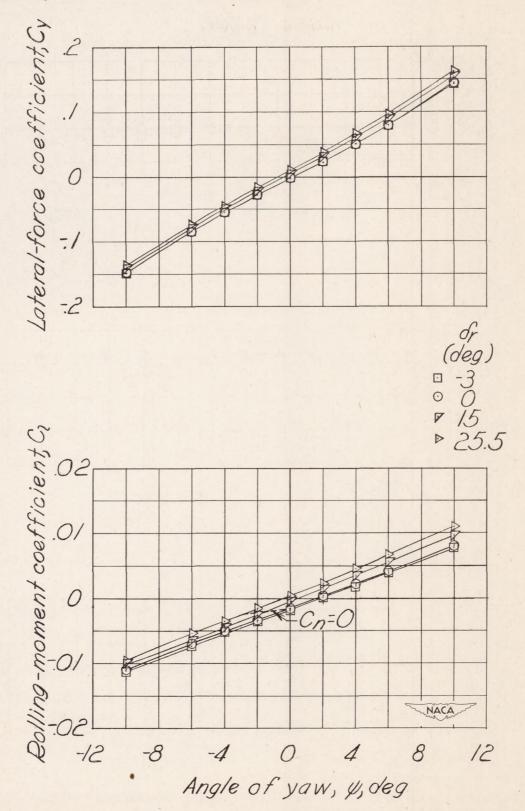
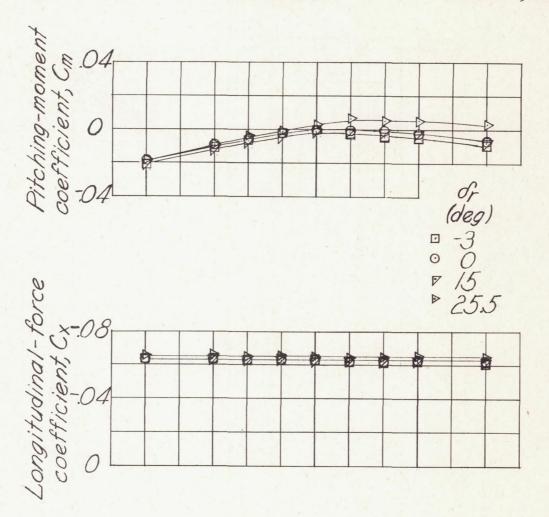


Figure 11. - Continued.



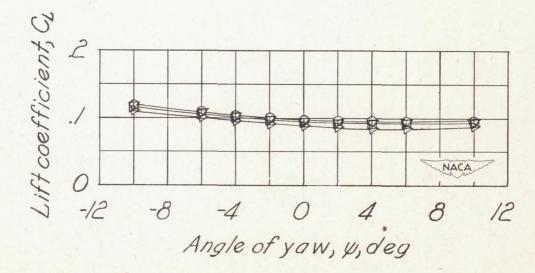


Figure 11. - Concluded.

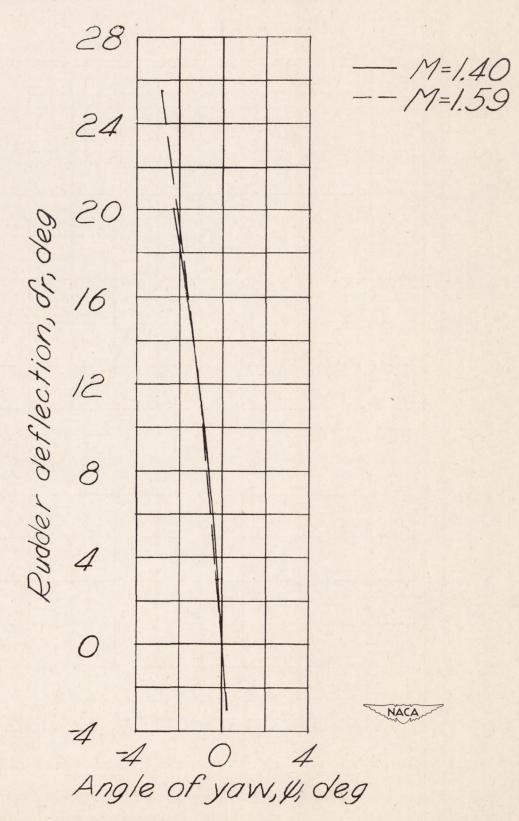


Figure 12.- Variation of rudder deflection with angle of yaw. C_{n}

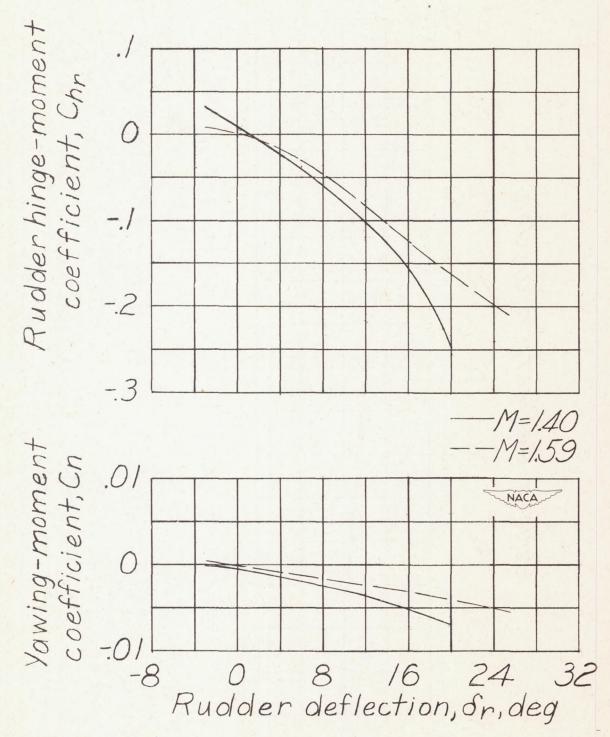


Figure 13.- Variation of yawing-moment and rudder hinge-moment coefficients with rudder deflection. $\psi = 0^{\circ}$.